EQUIVALENCE OF MATRIX MODELS FOR COMPLEX QCD DIRAC SPECTRA*

G. Akemann

Service de Physique Théorique CEA/Saclay
Unité associée CNRS/SPM/URA 2306
F-91191 Gif-sur-Yvette Cedex, France

(Received August 5, 2003)

Two different matrix models for QCD with a non-vanishing quark chemical potential are shown to be equivalent by mapping the corresponding partition functions. The equivalence holds in the phase with broken chiral symmetry. It is exact in the limit of weak non-Hermiticity, where the chemical potential squared is rescaled with the volume. At strong non-Hermiticity it holds only for small chemical potential. The first model proposed by Stephanov is directly related to QCD and allows to analyze the QCD phase diagram. In the second model suggested by the author all microscopic spectral correlation functions of complex Dirac operators can be calculated in the broken phase. We briefly compare those predictions to complex Dirac eigenvalues from quenched QCD lattice simulations.

PACS numbers: 12.38.Lg, 11.30.Rd, 05.40.–a

1. Introduction

Ten years ago the proposal [1] was made to use random matrix models in the study of the low energy phase of Quantum Chromodynamics (QCD), and it has turned out to be very successful. Since then many new matrix model correlation functions have been calculated for that purpose. The field theoretic origin for the applicability of matrix models has been understood and a wealth of data from QCD lattice simulations has been compared to their predictions. We refer the reader to [2] for a review summarizing these developments. However, the introduction of a chemical potential μ for quarks has left many open questions until very recently, concerning both numerical simulations as well as analytical matrix model predictions. The reason is that for non-vanishing μ the eigenvalues and thus the determinant of the Dirac operator become complex.

* Presented at the Workshop on Random Geometry, Kraków, Poland, May 15–17, 2003.

Let us summarize what can be calculated using random matrix models for QCD. The predictions can be put in two groups: the Dirac operator spectrum and the phase diagram. In the first case the distribution of Dirac eigenvalues λ_i rescaled with the volume V, $V\lambda_i = \text{const.}$, are predicted from matrix models close to the origin $\lambda = 0$. This region is magnified microscopically as it is most sensitive to spontaneous chiral symmetry breaking. This fact can be seen from the Banks–Casher relation, $\rho(0) = V\langle\bar{q}q\rangle/\pi$, which relates the Dirac operator spectral density $\rho(\lambda)$ at the origin to the order parameter for chiral symmetry breaking $\langle\bar{q}q\rangle$, the chiral condensate. The predictions of matrix models are universal and depend only the N_f quark flavors, their masses m_f, the topological charge and the global symmetry breaking pattern. They can be related to a particular limit of chiral perturbation theory, in which only the zero momentum modes of the Goldstone bosons contribute. The matrix model description breaks down at the Thouless energy, when non-zero momentum modes come into play.

In the second application matrix models are used as an effective model for QCD to predict the qualitative features of the phase diagram. The order and location of the phase transition lines is found by inspecting the non-analyticities of the matrix model partition function in terms of parameters as the temperature T and chemical potential μ. Here, the close relation to field theory is lost and the matrix model resembles a Landau–Ginsburg description. The following result was obtained in [3] for QCD with two massless quark flavors. A first order (full) line starting at large μ merges

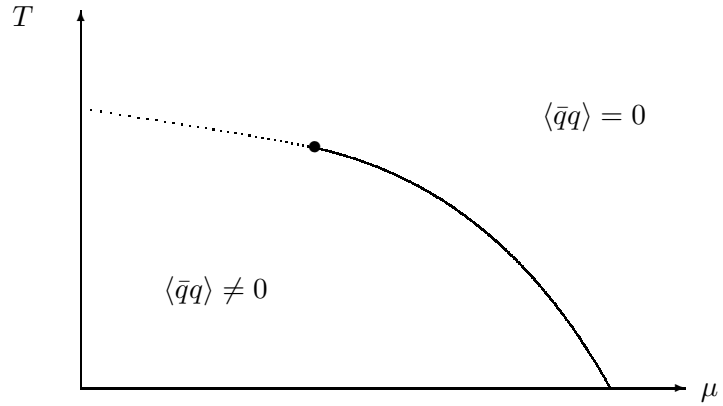

Fig. 1. The schematic QCD phase diagram with $N_f = 2$ massless flavors from [3].

with a second order (dotted) line from $\mu = 0$ into a tri-critical point. Other transitions from nuclear matter formation or more complicated phases such as color super-conductivity have been omitted here, where the latter can be addressed using matrix models as well [4].

We take this simplified phase diagram to explain which regions are explored. One part of the phase diagram accessible to QCD lattice simulations for three colors is the temperature axis at $\mu = 0$ (including more flavors and the influence of their mass ratio). The second part is for small values of μ in the vicinity of the second order phase transition line up to or crossing the tri-critical point. Only in the quenched approximation the full diagram can be covered so far. We refer to [5] for reviews and references. On the other hand very detailed matrix model predictions for the microscopic Dirac spectrum are available at $T = \mu = 0$ (see [2] and references therein). For $T \neq 0$ and $\mu = 0$ analytic predictions exist too [6,7] and have been compared to lattice simulations along the T-axis up to and above the transition [8].

Here, we will investigate the μ-axis at $T = 0$ instead, for which two different matrix models have been suggested [9,10]. The model introduced first by Stephanov [9] explicitly includes a chemical potential, using the same symmetry arguments as [1]. However, in this model only global properties are available, with the microscopic spectrum being unknown. For that reason another model [10] was proposed where all microscopic spectral correlators can be calculated. This model is only valid in the broken phase by construction. It follows from [1] by analytic continuation of the corresponding orthogonal polynomials into the complex plane and contains μ only implicitly through a non-Hermiticity parameter τ. Our aim here is to show that [10] is equivalent to [9] and thus as closely related to QCD. We prove that the two partition functions of these models are equal in the broken phase in the limit of infinite matrix size. In the limit of weak non-Hermiticity, keeping $V\mu^2$ fixed, the equivalence is shown for $N_f = 1, 2$ and 3 mass-degenerate flavors (the case of general N_f and $\nu \neq 0$ will be treated elsewhere [11]). At strong non-Hermiticity the partition functions are mapped for $N_f = 1$ to leading order in small μ, and we expect the equivalence to hold also for $N_f \geq 2$. The equality of partition functions does not automatically imply that all correlation functions are identical as well. However, it makes it very plausible that the results for the microscopic spectrum [10] are common to both models and are universal. We also give a brief comparison between the predictions [10] and quenched QCD lattice simulations [12, 13] for small $\mu \neq 0$ in the broken phase.

2. Equivalence of matrix models for QCD with $\mu \neq 0$

The following matrix model was introduced by Stephanov [9] to study QCD with chemical potential

$$\mathcal{Z}_{\rm I}(\mu; \{m_f\}) \equiv \int d\Phi \prod_{f=1}^{N_f} \det \begin{pmatrix} m_f & i\Phi + \mu \\ i\Phi^\dagger + \mu & m_f \end{pmatrix} \exp[-N\langle\bar{q}q\rangle^2 \,\mathrm{Tr}\, \Phi^\dagger \Phi] \,. \qquad (1)$$

Here Φ is a complex matrix of size $N \times (N+\nu)$ with the partition function being in the sector of topological charge ν. The quark masses m_f of the N_f flavors have to be rescaled with the volume in the same way as the eigenvalues in the microscopic limit. The block structure of the Dirac matrix follows from chiral symmetry and the location of μ is dictated by adding $\mu q^\dagger q$ to the quark Lagrangian. The Gaussian weight is chosen such that the Banks–Casher relation for $\mu = 0$ is satisfied. In the following we will mostly set $\langle \bar{q}q \rangle = 1$ for simplicity.

The partition function for $N_f = 1$ quark flavor was already know [14],

$$\mathcal{Z}_{\rm I}(\mu; m) \;=\; \exp[-N(1+\mu^2)] \exp[-Nm^2] \; I_0\left(2Nm\sqrt{1+\mu^2}\right) , \quad (2)$$

where I_0 denotes the modified Bessel function. Here we have taken already the large-N limit, assuming that the mass has to be rescaled with an appropriate power of the volume $V = 2N$ (see Eqs. (15), (23)). Eq. (2) holds in the broken phase. At a critical chemical potential $\mu_{\rm c} \approx 0.527$ determined by the equation [14]

$$1 + \mu_{\rm c}^2 + \log \mu_{\rm c}^2 \;=\; 0 \, , \quad (3)$$

a first order phase transition takes place. Above $\mu > \mu_{\rm c}$ it holds $\mathcal{Z}_{\rm I}(\mu; m) \sim \mu^{2N}$ for $m = 0$ [14]. This can be show by mapping Eq. (1) to a sigma model partition function over complex matrices σ of size $N_f \times N_f$ in Eq. (17), allowing us to treat also $N_f > 1$ in the broken phase below. The macroscopic spectral density of complex eigenvalues $z = x + iy$ given by [9]

$$\rho(z; \mu) = \frac{1}{4\pi} \left(\frac{\mu^2 + y^2}{(\mu^2 - y^2)^2} - 1 \right) , \quad (4)$$

is bounded by the following curve

$$0 = y^4(x^2 + 4\mu^2) \;+\; y^2(1 + 2\mu^2(2 - x^2 - 4\mu^2)) \;+\; \mu^4(x^2 - 4(1-\mu^2)) \, . \quad (5)$$

It splits into two domains only at $\mu = 1 > \mu_{\rm c}$. On the other hand for small $\mu \ll 1$ the density simplifies to a constant on an ellipse

$$\rho(z; \mu) = \frac{1}{4\pi\mu^2} \, , \quad \text{if} \quad \frac{x^2}{4} + \frac{y^2}{4\mu^4} \leq 1 \, . \quad (6)$$

Let us compare this to the second model [10]. The quenched $N_f = 0$ partition function is defined as

$$\mathcal{Z}_{\rm II}(\tau) \;\equiv\; \int \prod_{j=1}^{N} \left(d^2 z_j \; w(z_j, z_j^*) \right) \left| \Delta_N(z^2) \right|^2 , \quad (7)$$

$$w(z, z^*) \;=\; |z|^{2\nu+1} \exp\left[-\frac{N}{1-\tau^2} \left(|z|^2 - \frac{\tau}{2}(z^2 + z^{2\,*}) \right) \right] , \quad (8)$$

given in terms of complex eigenvalues instead of matrices. The Vandermonde determinant is denoted by $\Delta_N(z^2) = \prod_{k>l}^{N}(z_k^2 - z_l^2)$. The parameter $\tau \in [0,1]$ labels the degree of non-Hermiticity interpolating between real and maximally complex eigenvalues for $\tau = 1$ and $\tau = 0$, respectively. The macroscopic density reads [1]

$$\rho(z;\tau) = \frac{1}{2\pi(1-\tau^2)}\,, \quad \text{if} \quad \frac{x^2}{2(1+\tau)^2} + \frac{y^2}{2(1-\tau)^2} \leq 1\,. \tag{9}$$

Identifying the two macroscopic densities Eqs. (6) and (9), which implies that to leading order in N all moments of the two models become equal, leads us to[1]

$$2\mu^2 \;\equiv\; (1-\tau^2)\,. \tag{10}$$

Clearly the model Eq. (7) is always in the broken phase as the density is constant on a single domain for all $\tau \in [0,1)$. Here, all microscopic k-point correlations functions can be explicitly calculated using the technique of orthogonal polynomials in the complex plane [10] (see *e.g.* Eqs. (27), (28) below). For that purpose we define the following complex Laguerre polynomials in monic normalization,

$$\tilde{P}_k^{(\nu)}(z) \;\equiv\; (-1)^k k! \left(\frac{2\tau}{N}\right)^k L_k^{(\nu)}\left(\frac{Nz^2}{2\tau}\right), \tag{11}$$

which are orthogonal with respect to the weight Eq. (8).

In order to compare to the partition function Eq. (1) above we also have to introduce mass terms here, which we do as follows:

$$\begin{aligned}\mathcal{Z}_{\rm II}(\tau;\{m_f\}) \;&\equiv\; \mathcal{Z}_{\rm II}(\tau)^{-1} \int \prod_{j=1}^{N} \left(d^2 z_j \; w(z_j, z_j^*) \prod_{f=1}^{N_f} (z_j^2 + m_f^2) \right) \left|\Delta_N(z^2)\right|^2 \\ &=\; \left\langle \prod_{j=1}^{N} \prod_{f=1}^{N_f} (z_j^2 + m_f^2) \right\rangle \,. \end{aligned} \tag{12}$$

Such an expectation value can be calculated using the theorem proved in [15] for characteristic polynomials. In our case it only contains orthogonal polynomials in monic normalization, and we obtain

$$\mathcal{Z}_{\rm II}(\tau;\{m_f\}) \sim \frac{\det_{k,l=1,\ldots,N_f}\left[\tau^{N+k-1} L_{N+k-1}^{(\nu)}\left(\frac{-Nm_l^2}{2\tau}\right)\right]}{\Delta_{N_f}(m^2)}\,. \tag{13}$$

[1] Note the missing factor 2 in the corresponding equations in [10].

Here, we only display the τ-dependent prefactors. The partition function defined in Eq. (12) is thus real as it should. From Eq. (13) we can take the large-N limit where one has to distinguish now two cases, weak and strong non-Hermiticity.

2.1. The weak non-Hermiticity limit

In the weak non-Hermiticity limit introduced by [16] (see also the recent review [17]) we take the Hermitian limit $\tau \to 1$ and the infinite volume limit $N \to \infty$ at the same time, keeping

$$N(1-\tau^2) \;=\; 2N\mu^2 \;\equiv\; \alpha^2 \tag{14}$$

finite. In this limit the macroscopic density Eq. (9) becomes localized on the real line while the microscopic correlations functions still extend into the complex plane. In the microscopic limit we have to rescale the eigenvalues and consequently also the masses with the volume. In order to obtain a parameter free prediction this is done by

$$2N\langle\bar{q}q\rangle z \;=\; \xi\,, \tag{15}$$

and similarly for the masses. Since in the limit $\tau \to 1$ the model Eq. (7) has $\langle\bar{q}q\rangle = 1/\sqrt{2}$ we defined the rescaled masses as $\sqrt{2}Nm_f = \omega_f$. Taking the asymptotic large-N limit of Eq. (13) in this way we obtain

$$\mathcal{Z}_{\rm II,weak}(\alpha;\{\omega_f\}) \sim \exp\left[-\frac{N_f}{2}\alpha^2\right] \frac{\det_{k,l=1,\ldots,N_f}\left[\omega_l^{k-1} I_{k-1+\nu}(\omega_l)\right]}{\Delta_{N_f}(\omega^2)}\,, \tag{16}$$

where we have used that $\tau^N \to \exp[-\alpha^2/2]$ from the weak limit Eq. (14). The expression Eq. (16) only differs from the finite volume partition function at $\mu = 0$ [18] by the α-dependent exponential prefactor.

In order to prove that the same results can be obtained from the matrix model partition function Eq. (1) we rewrite it in terms of the following σ-model representation [14]:

$$\mathcal{Z}_{\rm I}(\mu;m) \;=\; \int d\sigma\, \exp[-N\langle\bar{q}q\rangle^2\, {\rm Tr}\,\sigma\sigma^\dagger]\, \det\begin{pmatrix} \sigma+m & \mu \\ \mu & \sigma^\dagger+m \end{pmatrix}^N . \tag{17}$$

Here, we have restricted ourselves to mass-degenerate flavors and to the sector of topological charge $\nu = 0$. Compared to Eq. (1) N and N_f have interchanged rôles, as σ is now a complex $N_f \times N_f$ matrix. We show explicitly for $N_f = 2$ how to calculate the integral Eq. (17) by parameterizing σ. The

calculation for $N_f = 3$ then follows in a similar way. Any complex matrix σ can be written in the Schur decomposition

$$\sigma \;=\; U(Z+R)U^{-1}\;, \tag{18}$$

where U is unitary, Z =diag$(z_1,\ldots,z_{N_f})$ is a diagonal matrix containing the complex eigenvalues and R is a complex, strictly upper triangular matrix. For $N_f = 2$ we thus have two complex eigenvalues and R contains a single complex number. Setting $\langle\bar{q}q\rangle = 1$ we can write

$$\begin{aligned}
\mathcal{Z}_{\rm I}(\mu;m) \;&=\; \int d^2z_1\, d^2z_2\, d^2R\;\exp\left[-N(|z_1|^2+|z_2|^2+|R|^2)\right]\;|z_2-z_1|^2 \\
&\quad\times\det\begin{pmatrix} |z_1|^2+m(z_1+z_1^*)+m^2-\mu^2 & (z_1^*+m)R \\ R^*(z_1+m) & |z_2|^2+m(z_2+z_2^*)+m^2-\mu^2 \end{pmatrix}^N \\
&=\; \int_0^\infty dr_1 r_1 dr_2 r_2 d\rho\rho \int_{-\pi}^{\pi} d\varphi_1 d\varphi_2 d\phi\,[(r_1^2-\mu^2)(r_2^2-\mu^2)-\rho^2\mu^2]^N \\
&\quad\times\exp\left[-N(\Sigma_{j=1,2}(r_j^2-2r_jm\cos\varphi_j)+2m^2+\rho^2)\right] \\
&\quad\times\left(r_1^2+r_2^2-2r_1r_2(\cos\varphi_1\cos\varphi_2+\sin\varphi_1\sin\varphi_2)\right) \\
&=\; (2\pi)^3\int_0^\infty dr_1 r_1 dr_2 r_2 d\rho\rho\;[(r_1^2-\mu^2)(r_2^2-\mu^2)-\rho^2\mu^2]^N \\
&\quad\times\exp\left[-N(r_1^2+r_2^2+\rho^2+m^2)\right]\;[(r_1^2+r_2^2)I_0(2Nmr_1) \\
&\quad\times I_0(2Nmr_2)-2r_1r_2I_1(2Nmr_1)I_1(2Nmr_2)]\;.
\end{aligned} \tag{19}$$

In the first step we have applied the Schur decomposition, which leads to the Vandermonde determinant. In the second step we have changed variables, $z_j \to \tilde{z}_j = (x_j+m)+i\,y_j = r_j\exp[i\varphi_j]$ for $j=1,2$, introducing polar coordinates here and in $R = \rho\exp[i\phi]$. In the last step we have carried out the angular integrations. So far all steps are exact. Next we employ the scaling Eq. (14), $\mu^2 = \alpha^2/(2N)$. Consequently we can replace the first factor in the last equation above by an exponential

$$[(r_1^2-\mu^2)(r_2^2-\mu^2)-\rho^2\mu^2]^N \to (r_1r_2)^N\exp\left[-\frac{\alpha^2(\rho^2+r_1^2+r_2^2)}{2r_1^2r_2^2}\right], \tag{20}$$

using $\lim_{N\to\infty}(1-x/N)^N = \exp[-x]$. The integral over ρ thus reads:

$$\lim_{N\to\infty}\int_0^\infty d\rho\rho\ \exp[-N\rho^2]\ [(r_1^2-\mu^2)(r_2^2-\mu^2)-\rho^2\mu^2]^N$$
$$=\frac{(r_1^2r_2^2)^{N+1}}{2Nr_1^2r_2^2+\alpha^2}\exp\left[\frac{-\alpha^2(r_1^2+r_2^2)}{2r_1^2r_2^2}\right]. \tag{21}$$

If we neglect the subleading α^2 in the denominator on the right-hand side the remaining integrals over r_1 and r_2 in Eq. (19) completely factorize. We can thus investigate them separately using a saddle point approximation. Because of $\langle\bar{q}q\rangle = 1$ we rescale the mass here as $2Nm = \omega$. Neglecting higher orders in $1/N$ the saddle point is at $r^2_{j=1,2} = 1$. The two contributions containing the factors I_0 and I_1 can be written in the following form,

$$\mathcal{Z}_{\rm I,weak}(\alpha;\omega)\ \sim\ \exp\left[-\alpha^2\right]\left|\begin{array}{cc} I_0(\omega) & I_1(\omega) \\ I_1(\omega) & I_0(\omega)\end{array}\right|. \tag{22}$$

This is equivalent to Eq. (16) for $N_f = 2$, when taking the limit of degenerate masses there. In particular it justifies on the level of partition functions the identification Eq. (10) leading to the scaling Eq. (14). The same calculation can be easily done for $N_f = 3$, following the same lines as above. In fact, recently we managed to show in full generality that Eq. (17) leads to Eq. (16) for all N_f with non-degenerate masses and topological charge $\nu \neq 0$ [11].

2.2. The strong non-Hermiticity limit

In this limit $\tau \in [0, 1)$ and thus μ^2 are kept fixed while the large-N limit is taken. Therefore both macroscopic and microscopic correlators extend to the complex plane. The microscopic rescaling has to be modified, reading

$$\sqrt{2N}\langle\bar{q}q\rangle z\ =\ \xi \tag{23}$$

for the eigenvalues and masses. Because μ^2 does not scale with N, the saddle point analysis for $N_f = 2$ or more flavors is difficult, as can be seen from Eq. (19). We therefore restrict ourselves to the case $N_f = 1$, taking Eq. (2) as a starting point. If we rescale the mass according to Eq. (23), $\sqrt{2N}m = \omega$, and expand for small values of $\mu^2 \ll 1$, we obtain

$$\mathcal{Z}_{\rm I,strong}(\mu;\omega) = \exp[-N(1+\mu^2)]\exp\left[\frac{-\omega^2}{2}\right] I_0\left(\sqrt{2N}\omega(1+\tfrac{1}{2}\mu^2)\right). \tag{24}$$

The evaluation of the second partition function takes a little more care, starting from Eq. (13). Expressing the single Laguerre polynomial as an integral, we obtain

$$\begin{aligned}\mathcal{Z}_{\rm II}(\tau;m) &\sim \tau^N \exp\left[\frac{-Nm^2}{2\tau}\right] \int_0^\infty ds \exp[-Ns] s^N I_0\left(Nm\sqrt{\frac{2s}{\tau}}\right) \\ &\sim {\rm e}^{-N}\tau^N \exp\left[\frac{-Nm^2}{2\tau}\right] I_0\left(Nm\sqrt{\frac{2}{\tau}}\right). \end{aligned} \tag{25}$$

In the saddle point expansion is the second step we have already used the mass rescaling $\sqrt{N}m = \omega$, which is appropriate here for $\langle\bar{q}q\rangle^2 = 1/2$ with τ close to unity. If we employ again the relation (10), $\tau^2 = 1 - 2\mu^2$, insert it here and expand in $\mu^2 \ll 1$ we arrive at

$$\begin{aligned}\mathcal{Z}_{\rm II,strong}(\mu;\omega) &= \exp[-N(1+\mu^2)] \exp\left[\frac{-\omega^2}{2}(1+\mu^2)\right] \\ &\quad \times I_0\left(\sqrt{2N}\omega(1+\tfrac{1}{2}\mu^2)\right). \end{aligned} \tag{26}$$

We have used that $\tau^N \to \exp[-N\mu^2]$, omitting terms of order $O(\mu^4)$. We observe that the leading order (suppression) term in μ^2 as well as the term I_0 exponentially growing in ω match to the given order $O(\mu^2)$. We recall that the matching of the two macroscopic densities also included an expansion of Eq. (4) in μ^2 to obtain Eq. (6). The finite term $\exp[-\omega^2/2]$ only matches to zero-th order.

We find this mapping of the two partitions functions at strong non-Hermiticity quite remarkable and can show it to hold also for $N_f \geq 2$ and small $\mu^2 \ll 1$ [11]. Another reason for that is that the strong limit can be obtained from the weak limit in taking $\alpha \to \infty$. While the two partition functions may disagree for larger values of μ^2, as the expansions indicates, this does not exclude a universal behavior of the corresponding microscopic correlation functions. A mapping of these quantities may though include a nontrivial, μ- and τ-dependent unfolding procedure, respectively.

3. Comparison to lattice data

In this section we briefly recall the matrix model predictions [10] and their confirmation by quenched QCD lattice data [12]. A more detailed analysis of the data will be published elsewhere [13].

The quenched microscopic spectral density at weak non-Hermiticity in the sector of topological charge ν is given by

$$\rho_{\rm weak}(\xi) = \frac{\sqrt{\pi\alpha^2}}{{\rm erf}(\alpha)}\ |\xi|\ \exp\left[\frac{-1}{\alpha^2}(\Im m\,\xi)^2\right]\int_0^1 dt\ {\rm e}^{-\alpha^2 t} J_\nu(\sqrt{t}\xi)J_\nu(\sqrt{t}\xi^*)\,, \quad (27)$$

where the eigenvalues are rescaled according to Eq. (15). The density is normalized to unity for large arguments on the real line. At strong non-Hermiticity we obtain

$$\rho_{\rm strong}(\xi) = \sqrt{\frac{2\pi}{1-\tau^2}}\ |\xi|\ \exp\left[\frac{-|\xi|^2}{1-\tau^2}\right] I_\nu\left(\frac{|\xi|^2}{1-\tau^2}\right), \quad (28)$$

with the different rescaling Eq. (23). Higher order correlation functions can be found in [10].

The data we compare with were generated on a 6^4 lattice at gauge coupling $\beta = 5.0$. Since staggered fermions at strong coupling away from the continuum limit are topology blind as explained in [19], we have set $\nu = 0$ in all comparisons below. The two values chosen for the chemical potential are $\mu = 0.006$ and $\mu = 0.2$. They correspond to weak and strong non-Hermiticity, respectively. We display the same figures as in Ref. [12] but with more statistics (17.000 and 20.000 configurations, respectively). For simulations with other lattice sizes, confirming the scaling prediction Eq. (14) in the weak limit, we refer again to [13]. The data are rescaled

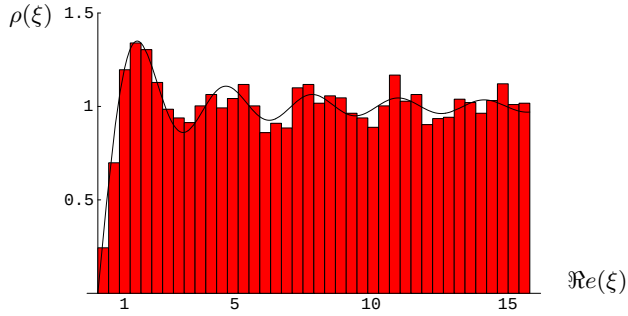

Fig. 2. Cut of the Dirac eigenvalue density along the real axis for $\mu = 0.006$.

with the mean level spacing $d \sim 1/V$ determined as follows. For $\mu = 0.006$ the data almost lie on the real axis and are therefore ordered according to their real part. We thus simply count the number of eigenvalues in a (real) interval of given length to determine the average spacing. The same factor d is used to rescale μ^2 from Eq. (14) and we obtain $\alpha = 0.19$. In Figs. 2 and 3

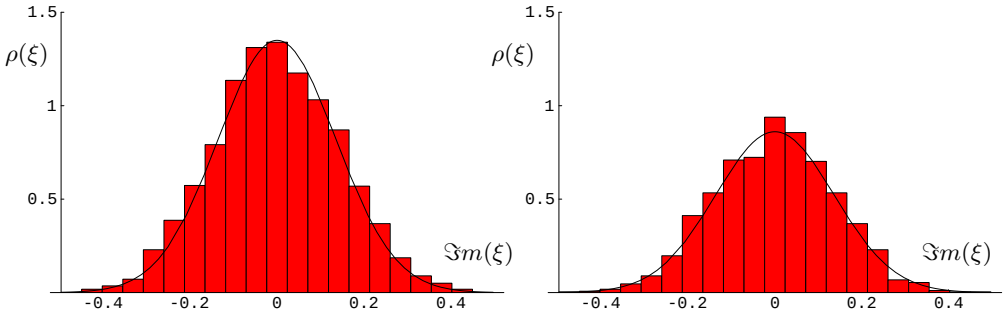

Fig. 3. Cuts of the same density along the imaginary axis, with fixed real part of the eigenvalues at the first maximum (left) and minimum (right) in Fig. 2.

Eq. (27) is plotted with this value of α *versus* the rescaled data, and we find an excellent agreement. We note that there are no free parameters and that no fit has been made[2]. Fig. 2 is very reminiscent to comparisons for $\mu = 0$ (see [2]), with the difference that we need at least 10 times more statistics. This is due to the spread of the data into the complex plane seen in Fig. 3, which is thus truly testing the value of α. Here, Eq. (27) is plotted for fixed real part $\Re e(\xi)$ on the first maximum and minimum (saddle) next to the origin. Comparing to the histograms that contain the maximum or minimum we find an excellent agreement. In [13] the same picture is confirmed for different lattice sizes keeping the value of α fixed.

At strong non-Hermiticity μ does not scale with the volume and we thus have $\tau = \sqrt{1-2\mu^2} \approx 0.96$ for $\mu = 0.2$. The data are rescaled with the inverse square root of the mean level spacing determined as follows. For this value of chemical potential the spreading of data into the complex plane is such that an ordering according to the real part does no longer make sense. For a given set of eigenvalues in our window close to the origin we thus determine for each eigenvalue its closest neighbor in the complex plane and then average over these distances. After averaging over all configurations we obtain the mean level spacing. In Fig. 4 left (right) the density Eq. (28) is plotted for fixed $\Re e(\xi) = 0$ ($\Im m(\xi) = 0$) and compared to the histograms along the imaginary (real) axis. We find very good agreement with the parameter free prediction[3]. The statistical fluctuations are still larger than in the weak limit, because for about the same number of configurations more eigenvalues have moved away from the real axis. Along the imaginary axis the density drops to zero already at $\sim \pm 1.1$ in given units, indicating that only part of the left histogram is truly in the microscopic regime.

[2] The correction of Eq. (10) explains the small discrepancy found in [12].

[3] We note that compared to [12] we have refined the determination of the level spacing. In addition Eq. (28) has been rescaled, taking properly into account $\langle \bar{q}q \rangle^2 = 1/2$.

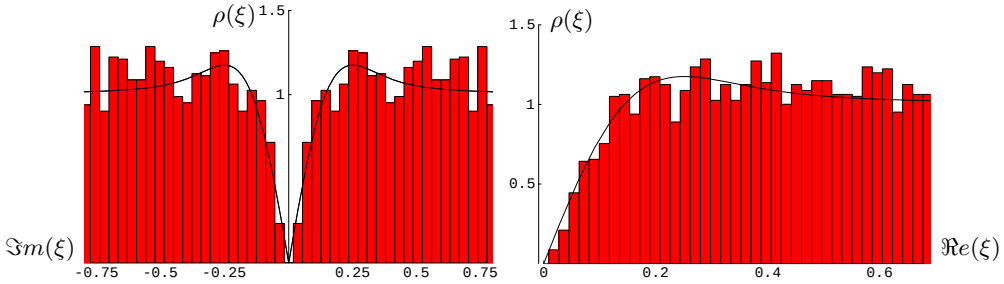

Fig. 4. Cuts of the Dirac eigenvalue density for $\mu = 0.2$ along the imaginary (left) and real axis (right).

4. Conclusions

To summarize we have shown the equivalence of two different matrix model realizations [9, 10] for QCD with chemical potential. The equivalence holds for weak non-Hermiticity with several flavors and for strong non-Hermiticity with at least one flavor for small chemical potential. It shows that the results of [10] can be directly related to QCD. To illustrate this we have compared to quenched QCD lattice data for the microscopic Dirac operator spectrum and found agreement in both limits, for weak and strong non-Hermiticity.

We close with some remarks on the quenched approximation. While the origin of its failure to describe QCD with non-vanishing chemical potential was clarified in [9], the matrix model is valid beyond the quenched approximation as well. It should be mentioned that also for zero chemical potential the quenched approximation is not without inconsistencies [20]. Nevertheless, matrix models do correctly describe unquenched simulations, as can be seen *e.g.* for two colors with dynamical fermions [21]. For complex spectra so far only quenched or phase quenched predictions with massless flavors are available [10]. In proving the equivalence we have learned how to introduce mass terms. This indicates that with a chemical potential the duality between massless flavors and topology proved in [22] may no longer hold in general. This seems quite plausible since for example the quenched theory with nonzero topology $\nu \neq 0$ should not carry a phase, while the unquenched theory with the same number of massless flavors N_f and zero topology should carry a phase.

I wish to thank Y. Fyodorov, G. Vernizzi and T. Wettig for collaboration and many fruitful discussions. This work was supported by a Heisenberg fellowship of the Deutsche Forschungsgemeinschaft and in part by the European network on "Discrete Random Geometries" HPRN-CT-1999-00161 (EUROGRID).

REFERENCES

[1] E.V. Shuryak, J.J.M. Verbaarschot, *Nucl. Phys.* **A560**, 306 (1993).

[2] J.J.M. Verbaarschot, T. Wettig, *Ann. Rev. Nucl. Part. Sci.* **50**, 343 (2000).

[3] M.A. Halasz, A.D. Jackson, R.E. Shrock, M.A. Stephanov, J.J.M. Verbaarschot, *Phys. Rev.* **D58**, 096007 (1998).

[4] B. Vanderheyden, A.D. Jackson, *Phys. Rev.* **D62**, 094010 (2000).

[5] J.B. Kogut, D.K. Sinclair, `hep-lat/0209054`; E. Laermann, O. Philipsen, `hep-ph/0303042`.

[6] T. Guhr, T. Wettig, *Nucl. Phys.* **B506**, 589 (1997); B. Seif, T. Wettig, T. Guhr, *Nucl. Phys.* **B548**, 475 (1999).

[7] R.A. Janik, M.A. Nowak, G. Papp, I. Zahed, *Phys. Lett.* **B446**, 9 (1999).

[8] F. Farchioni, Ph. de Forcrand, I. Hip, C.B. Lang, K. Splittorff, *Phys. Rev.* **D62**, 014503 (2000); P.H. Damgaard, U.M. Heller, R. Niclasen, K. Rummukainen, *Nucl. Phys.* **B583**, 347 (2000); E. Bittner, M.-P. Lombardo, H. Markum, R. Pullirsch, *Nucl. Phys. Proc. Suppl.* **106**, 468 (2002).

[9] M.A. Stephanov, *Phys. Rev. Lett.* **76**, 4472 (1996).

[10] G. Akemann, *Phys. Rev. Lett.* **89**, 072002 (2002); *J. Phys.* **A***: Math. Gen.* **36**, 3363 (2003).

[11] G. Akemann, Y.V. Fyodorov, G. Vernizzi, in preparation.

[12] G. Akemann, T. Wettig, proceedings of "Strong and Electroweak Matter 2002", ed. M.G. Schmidt, World Scientific 2003.

[13] G. Akemann, T. Wettig, `hep-lat/0308003`.

[14] M.A. Halasz, A.D. Jackson, J.J.M. Verbaarschot, *Phys. Rev.* **D56**, 5140 (1997).

[15] G. Akemann, G. Vernizzi *Nucl. Phys.* **B660**, 532 (2003).

[16] Y.V. Fyodorov, B.A. Khoruzhenko, H.-J. Sommers, *Phys. Lett.* **A226**, 46 (1997); *Phys. Rev. Lett.* **79**, 557 (1997).

[17] Y.V. Fyodorov, H.-J. Sommers, *J. Phys.* **A36**, 3303 (2003).

[18] H. Leutwyler, A. Smilga, *Phys. Rev.* **D46**, 5607 (1992); R. Brower, P. Rossi, C.-I. Tan, *Nucl. Phys.* **B190**, 699 (1981); A.D. Jackson, M.K. Şener, J.J.M. Verbaarschot, *Phys. Lett.* **B387**, 355 (1996).

[19] P.H. Damgaard, *Nucl. Phys.* **B608**, 162 (2001).

[20] P.H. Damgaard, *Nucl. Phys.* **B556**, 327 (1999).

[21] M.E. Berbenni-Bitsch, S. Meyer, T. Wettig, *Phys. Rev.* **D58**, 071502 (1998); G. Akemann, E. Kanzieper, *Phys. Rev. Lett.* **85**, 1174 (2000).

[22] G. Akemann, D. Dalmazi, P.H. Damgaard, J.J.M. Verbaarschot, *Nucl. Phys.* **B601**, 77 (2001); D. Dalmazi, J.J.M. Verbaarschot, *Phys. Rev.* **D64**, 054002 (2001).